

1 **Article Type:** Short Communication

2 **Northward shift of the southern westerlies during the Antarctic Cold Reversal**

3 **Authors:** Fletcher, Michael-Shawn<sup>1,2\*</sup>, Pedro, Joel<sup>3,4</sup>, Hall, Tegan<sup>1</sup>, Mariani, Michela<sup>1,5</sup>, Alexander, Jo-  
4 seph A.<sup>1</sup>, Beck, Kristen<sup>1,6</sup>, Blaauw, Maarten<sup>7</sup>, Hodgson, Dominic A.<sup>8</sup>, Heijnis, Henk<sup>9</sup>, Gadd, Patricia. S.<sup>9</sup>,  
5 Lise-Pronovost, Agathe<sup>10</sup>

6

7 **Affiliations:**

8 <sup>1</sup>School of Geography, University of Melbourne, Victoria, Australia

9 <sup>2</sup>Indigenous Knowledge Institute, University of Melbourne, Victoria, Australia

10 <sup>3</sup>Australian Antarctic Division (AAD), Kingston, Tasmania, Australia

11 <sup>4</sup>Australian Antarctic Program Partnership, Institute for Marine and Antarctic Studies, University of  
12 Tasmania, Hobart, Tasmania

13 <sup>5</sup>School of Geography, University of Nottingham, Nottingham, United Kingdom

14 <sup>6</sup>Lincoln Centre for Water and Planetary Health, School of Geography, University of Lincoln, Lincoln,  
15 United Kingdom

16 <sup>7</sup>School of Natural and Built Environment, Queen's University Belfast, United Kingdom

17 <sup>8</sup>British Antarctic Survey, Cambridge & Department of Geography, Durham University, United King-  
18 dom

19 <sup>9</sup>Australian Nuclear Science and Technology Organisation, New South Wales, Australia

20 <sup>10</sup>School of Earth Sciences, University of Melbourne, Victoria, Australia

21 \*Corresponding author: michael.fletcher@unimelb.edu.au

22 **Abstract:** Inter-hemispheric asynchrony of climate change through the last deglaciation has been  
23 theoretically linked to latitudinal shifts in the southern westerlies via their influence over CO<sub>2</sub> out-  
24 gassing from the Southern Ocean. Proxy-based reconstructions disagree on the behaviour of the  
25 westerlies through this interval. The last deglaciation was interrupted in the Southern Hemisphere by  
26 the Antarctic Cold Reversal (ACR; 14.7 to 13.0 ka BP (thousand years Before Present)), a millennial-  
27 scale cooling event that coincided with the Bølling–Allerød warm phase in the North Atlantic (BA; 14.7  
28 to 12.7 ka BP). We present terrestrial proxy palaeoclimate data that demonstrate a migration of the  
29 westerlies during the last deglaciation. We support the hypothesis that wind-driven out-gassing of old  
30 CO<sub>2</sub> from the Southern Ocean drove the deglacial rise in atmospheric CO<sub>2</sub>.

31 **Highlights:**

32 We present empirical palaeoclimate data that demonstrate a northward shift of the southern westerly  
33 wind during the Antarctic Cold Reversal (ACR) that drove antiphase west-east environmental  
34 responses across the island of Tasmania.

35 Stronger westerly wind flow over Tasmania during the ACR drove wetter conditions on the western  
36 (windward) slopes of the Tasmanian mountains that dampened regional fire activity and drove  
37 regional vegetation change toward more cold tolerant plant communities.

38 Stronger westerly wind flow over Tasmania during the ACR drove increased evaporation on the  
39 eastern (leeward) side of the Tasmanian mountains.

40 Our results support that millennial scale climate variability involves global reorganisation of ocean  
41 and atmospheric circulation and heat transport.

42

## 43 **1.0 Introduction**

44 The southern westerlies are part of a zonally-symmetric system that dominates the climate of the mid-  
45 to high-latitudes of the Southern Hemisphere (Garreaud, 2007). Changes in the strength and  
46 latitudinal position of the southern westerlies are believed to modulate global atmospheric CO<sub>2</sub>  
47 concentration via changes in wind stress over the Southern Ocean. Wind stress influences the  
48 upwelling of CO<sub>2</sub> saturated deep waters and the capacity of the surface ocean to absorb, or release,  
49 CO<sub>2</sub> (Siani et al., 2013). In the ocean, the latitudinal position of the southern westerlies is linked to the  
50 position of the Subpolar Oceanic Front and the Antarctic Circumpolar Current (Toggweiler et al., 2006),  
51 while on land changes in the southern westerlies govern mid- to high-latitude terrestrial climate,  
52 principally hydroclimate (Garreaud, 2007), which has a profound influence over a range of terrestrial  
53 processes (Fletcher and Moreno, 2012; Mariani and Fletcher, 2017). Parallel latitudinal shifts of the  
54 southern westerlies and Intertropical Convergence Zone (ITCZ) have also been proposed for the last  
55 deglaciation as part of the atmospheric response to changes in ocean heat transport by the Atlantic  
56 Meridional Overturning Circulation (AMOC) (Buizert et al., 2018; Denton et al., 2010; Markle et al.,  
57 2017; Pedro et al., 2016; Sigman et al., 2020). However, while proxy data confirm a cooling in the mid-  
58 to high latitudes of the Southern Hemisphere (poleward of ca. 40°S) during the ACR, in palaeoclimate  
59 proxy data provide no clear constraint on the latitudinal behaviour of the southern westerlies through  
60 this interval.

61 We reconstruct westerly wind behaviour in the mid-latitudes of the Australian sector of the Southern  
62 Hemisphere from multiproxy data from six radiocarbon-dated lake sediment sequences from  
63 Tasmania (40-44°S; Figure 1a). Tasmania is uniquely situated to investigate the behaviour of the  
64 southern westerlies during the ACR due to its location at the northern margins of the westerly wind  
65 belt and an exceptionally strong correlation between southern westerly wind speed and its rainfall  
66 anomalies (Figure 1b) (Gillett et al., 2006). This means that rainfall proxies can be applied to  
67 reconstruct past changes in wind regimes. Tasmania's mountainous west coast and contrasting

68 lowland east coast create an orographic effect that splits the island into clear zones of positive  
69 (western sites) and negative (eastern sites) correlation between southern westerly wind speed and  
70 rainfall (Figure 1b). This allows us to target sites where there is an unambiguous southern westerly  
71 influence over rainfall.

72 We compile new lake sediment rainfall proxies including charcoal, pollen and geochemistry from six  
73 lakes located in zones of both significant positive and significant negative correlation between  
74 southern westerly wind speed and rainfall (Figure 1b). While the charcoal proxy is influenced by  
75 human-caused fire ignitions (Bowman and Brown, 1986), the occurrence and spread of fires is  
76 moisture-limited in the high-rainfall west of Tasmania (McWethy et al., 2013; Styger and Kirkpatrick,  
77 2015). Sedimentary charcoal analyses have previously revealed a coherence between changes in  
78 regional charcoal (biomass burning) and changes in moisture delivery by the southern westerlies  
79 through the Holocene: increased southern westerly flow over Tasmania results in reduced  
80 sedimentary charcoal content (and vice-versa), reflecting the primacy of southern westerly-derived  
81 orographic rainfall over regional fire regimes (Mariani and Fletcher, 2017; Mariani and Fletcher, 2016).

82

## 83 **2.0 Material and methods**

### 84 *2.1 Construction of age models*

85 <sup>14</sup>C analysis using accelerator mass spectrometry (AMS) was used to date each sediment record  
86 utilised in this analysis. Results for each sample submitted for analysis, along with their calibrated age  
87 ranges, are provided in Table 1. All radiocarbon ages were calibrated using SHCal20 (Hogg et al., 2020)  
88 and age-depth models for each core (Figure 3) were constructed using the *rbacon* v2.3.9.1 (Blaauw  
89 and Christen, 2011) package in R. Modelling was restricted to ~9 to 18 kya. Modelled age outputs were  
90 then used to compare regional proxy data records.

### 91 *2.2 Palaeofire compilation*

92 Palaeofire analysis was carried out using the paleofire package in R (Blarquez et al., 2014) and follows  
93 the methodology outlined in Mariani & Fletcher (2016). Three charcoal records from the precipitation-  
94 dominant western Tasmania were considered for this analysis (Lake Selina, Basin Lake and Lake Vera).  
95 Firstly, a transformation of the data was performed using the function pfTransform with MinMax, Box-  
96 Cox and Z-score methods. Transformation and standardization of different charcoal records is a highly  
97 recommended step in generating a synthesis (Blarquez et al., 2014). Here, we used the methodology  
98 proposed by Power et al. (2008) and involved a three-step data transformation including a min-max  
99 data-rescaling, variance homogenization using Box-Cox data transformation (Box and Cox, 1964), and  
100 final rescaling to Z-scores. The palaeofire composite was calculated using the function pfCompositeLF,  
101 consisting in a modified version of existing methods (Daniau et al., 2012; Marlon et al., 2008), involving  
102 a two-stage smoothing method (including LOWESS; Cleveland, 1979) of the selected bins interval. In  
103 this case, 100 years-bins were used, since it represents the best achievable resolution in order to  
104 include the majority of charcoal records for the entire reconstruction period. Confidence intervals  
105 were obtained using the function circboot with 1000 repetitions, which applies a "moving" or  
106 "circular" block bootstrap method (Kunsch, 1989) to test significance of changes in stationary time  
107 series.

### 108 **2.3 Geochemical proxy analysis**

109 Micro-X-Ray fluorescence spectrometry ( $\mu$ XRF) elemental profiles were obtained for three western  
110 Tasmanian records (Lake Tiberias, Lake Selina and Hazards Lagoon from the Australian Nuclear Science  
111 and Technology Organisation (ANSTO)). Cores were scanned at 0.5 mm resolution using Cox Analytical  
112 Systems ITRAX  $\mu$ XRF core scanner with a Mo tube (55mA current; 20s count time; 30kV voltage). Raw  
113 data were normalised to kpcs (Croudace and Rothwell, 2015). Ca/Ti ratios for each record were  
114 extracted from the full dataset as a proxy for relative evaporation levels across western Tasmania  
115 (Croudace and Rothwell, 2015).

116 The geochemistry of lake sediments is also influenced by changes to in-lake processes such as  
117 evaporative conditions and lake levels. The deposition of evaporative carbonate minerals into lake  
118 sediments is influenced by authigenic (within-lake) and allogenic (external catchment) processes,  
119 making it necessary to isolate the signal of authigenic deposition in order to infer changes to in-lake  
120 conditions (Cohen, 2003). For example, by normalising  $\mu$ XRF carbonate proxy elements (calcium and  
121 strontium) against stable detrital elements in the record, it is possible to isolate the authigenic  
122 carbonate signal (Croudace & Rothwell, 2015). This method has been widely used in paleolimnology,  
123 including in western Tasmania (Fletcher et al., 2014), and forms the basis for interpretations of in-lake  
124 conditions at Lake Rolleston. Precipitation of evaporative carbonate minerals in fresh-water lakes  
125 varies with changes to evaporative conditions and lake levels (Cohen, 2003; Haberzettl et al., 2007;  
126 Kelts and Hsü, 1978). The type of evaporative minerals that are precipitated in the water column are  
127 dependent on initial water chemistry, which is related to the underlying catchment geology (Eugster  
128 and Hardie, 1978).

#### 129 **2.4 Palynology**

130 Pollen samples were prepared and analysed for the four western Tasmanian sites (Basin Lake, Lake  
131 Vera, Paddy's Lake and Lake Selina) according to standard protocols (Faegri and Iversen, 1989).  
132 Percentages of *Phyllocladus aspleniifolius* and Poaceae taxa were isolated from the full pollen  
133 datasets, focusing on the last 18kya. Raw percentage data for these taxa were calculated from the  
134 terrestrial pollen sum and are presented in Figures S4 (*P. aspleniifolius*) and S5 (Poaceae). Data from  
135 all six sites were then collated into one time series to construct a regional time-series for each taxon.  
136 Prior to collation, data were standardised (transformed into z-scores) to account for differences in the  
137 mean abundances of the original datasets.

138

#### 139 **3.0 Results**

140 All graphed results are in the Supplementary Information (Figs. S1-5) and this section only briefly  
141 describes the results here. All selected cores span the ACR interval with sufficient dating to resolve  
142 environmental changes through this interval (Figure S1). Synthesis of the charcoal records from the  
143 western Tasmanian sites (n=4) demonstrates a sharp increase in CHAR across the west commencing  
144 at ca. 17.8 ka BP and continuing until ca. 15 ka BP, before declining between ca. 13.5 ka BP. CHAR  
145 values rise again toward peak regional values at ca. 12.2 ka BP and decline thereafter (Figs 2, S3).  
146 Calculation of the Ca/Ti ratio for the evaporation-dominant sites in eastern Tasmania show a discrete  
147 peak in overall values during the ACR interval (ca. 14.7 to 13.0 ka BP) indicating a peak in calcite  
148 precipitation under evaporative conditions during this interval (Figure 2). The synthesised pollen  
149 records from the precipitation-dominant western Tasmanian sites show increased values in the  
150 hygrophilous conifer *P. aspleniifolius* between ca. 16-12 ka BP, with a discrete dip centred on the ACR  
151 interval (Figure S4). High Poaceae values, associated with cool temperatures in western Tasmania  
152 (Fletcher and Thomas, 2007), occur discretely during the ACR interval, embedded in a long-term  
153 decrease commencing at ca. 18 ka BP (Figure S5).

154

#### 155 **4.0 Discussion**

156 Charcoal influx to the western Tasmanian lakes decreases during the ACR (Figs. 2d, S2-3), consistent  
157 with enhanced westerly winds and rainfall, reducing biomass burning. This change is synchronous with  
158 a marked increase in carbonate precipitation and subsequent deposition (sedimentary Ca/Ti ratio)  
159 (Kylander et al., 2011) at two sites in eastern Tasmania (Figs. 2a,b) and a concomitant decrease in  
160 carbonate deposition in the west (Figure 2c). Carbonate precipitation occurs under increased  
161 evaporative conditions in freshwater lakes (Kelts and Hsü, 1978) and the east-west anti-phasing of  
162 carbonate deposition displayed in our data during the ACR mirrors the modern rainfall-southern  
163 westerly relationship (Figure 1), suggesting an increase in wind speed over Tasmania at this time. The  
164 increasing sedimentary charcoal in the west of Tasmania immediately prior to (ca. 17-15 ka BP) and

165 following (>13 ka BP) the ACR (Figure 2d) is consistent with a drier climate under a weaker southern  
166 westerly flow. These trends in proxy-inferred hydroclimate across Tasmania indicate either a  
167 strengthening of the westerly flow at their northern edge or a northward displacement of the  
168 westerlies during the ACR. The modern zone of maximum westerly winds speed lies between 50-60°S  
169 (Garreaud et al., 2009). A reduction in westerly wind-driven upwelling at marine core site TN057-13PC  
170 (located at 53.2°S, 5.1°E; Figure 1a) on the southern edge of the southern westerlies during the ACR  
171 (Anderson et al., 2009) (Figure 3g) is synchronous with our inference of an increase in westerly flow  
172 at their northern edge in Tasmania (see Supplementary Information Table S1). This synchronicity of  
173 the ACR signal across the Southern Hemisphere suggests that a northward shift in the Australian sector  
174 is more likely than a stationary strengthening.

175

176 Our composite pollen data (see Figs. S4-5) from across western Tasmania indicate a regional expansion  
177 of Poaceae pollen (indicative of grassland; Figure 2f) during the ACR at the expense of *Phyllocladus*  
178 *aspleniifolius* (Figure 2e), a lowland temperate rainforest tree. Forests replaced grasslands during the  
179 last deglaciation in Tasmania in response to increasing temperature (Colhoun, 2000; Fletcher and  
180 Thomas, 2010), and our pollen data reflect a short-lived reversal of this trend in response to a  
181 temperature decrease during the ACR. Cooling over Tasmania is supported by proxy and model-based  
182 reconstructions of the ACR across the mid- to high-latitudes of the Southern Hemisphere (Koffman et  
183 al., 2017; Pedro et al., 2016; Putnam et al., 2010; Vandergoes et al., 2008). Collectively, our data  
184 indicate reduced temperature and increased southern westerly flow over Tasmania during the ACR  
185 that resulted in a cool and wet climate on the mountainous west coast sites, and a cool and dry climate  
186 on the lowland east coast sites.

187

188 We observe a synchronous and in-phase relationship between southern westerly changes over  
189 Tasmania and changes in the strength of the Leeuwin Current (De Deckker et al., 2012) (inferred from



190 core MD03-2611 in the Great Australian Bight; Figure1a), a surface ocean current that delivers warm  
191 tropical water from the Indo-Pacific Warm Pool to southern Australia (carrying tropical foraminifera  
192 such as *Globigerinoides ruber*) (Figure 3d) (Weaver and Middleton, 1989). The Leeuwin current is  
193 strongest in the Austral winter, when the northerly displaced southern westerlies accelerate the  
194 current along Australia's southern coast (Cirano and Middleton, 2004). We suggest the increased  
195 proportion of tropical foraminifera observed in MD03-2611 during the ACR can be explained by a  
196 northward-shifted southern westerly wind flow over the Australian sector. This shift would strengthen  
197 the Leeuwin Current along the south coast of Australia, in a similar way as seasonal migrations of the  
198 southern westerlies do today (Figure 3d).

199

200 Northward migration of the southern westerlies during the ACR is consistent, from an atmospheric  
201 dynamics perspective, with the documented northward shift of the ITCZ over northern Australia  
202 (Ayliffe et al., 2013; Ceppi et al., 2013; Denniston et al., 2013). The tendency for the ITCZ and southern  
203 westerlies to shift in the same direction is explained in detail elsewhere (Ceppi et al., 2013; Lee et al.,  
204 2011) and is documented by empirical data in the Australian sector during the Holocene (Mariani et  
205 al., 2018). In brief, a northward shift of the ITCZ is associated with strengthening of the Southern  
206 Hemisphere Hadley circulation delivering increased heat and eddy-momentum flux into the Southern  
207 Hemisphere subtropics. The increased momentum flux strengthens the subtropical jet and pulls the  
208 eddy driven jet (of which the surface expression is the southern westerlies) northward (Ayliffe et al.,  
209 2013; Denniston et al., 2013; Ceppi et al., 2013; Chiang et al., 2014) (Figure 6).

210

211 Importantly, our interpretation reconciles southern westerly proxy data spanning the ACR in the  
212 Australian region (De Deckker et al., 2012) with southern westerly behaviour elsewhere in the  
213 Southern Hemisphere. Rainforest declines in northeastern Brazil and the expansion of Magellanic  
214 moorland in western Patagonia indicate a northward shift in both the ITCZ and southern westerlies

215 between 15-13 ka BP (Montade et al., 2015). Recent Antarctic ice core based evidence show zonal  
216 shifts in moisture sources that similarly indicate northward movement of the westerlies during the  
217 ACR as well as earlier abrupt glacial climate changes (Buizert et al., 2018; Markle et al., 2017).

218 Our results provide further empirical evidence for the dynamics-based view that millennial scale  
219 climate variability involves major global reorganisation of ocean and atmospheric circulation and heat  
220 transport (Buizert et al., 2018; Markle et al., 2017; Pedro et al., 2016). The much-cited thermal ocean  
221 seesaw mechanism (Stocker and Johnson, 2003) is only one component of this larger coupled ocean-  
222 atmosphere reorganisation. Enhanced northward ocean heat transport is the primary energy source  
223 sustaining the Northern Hemisphere warming of the Bølling-Allerød and the South Atlantic and  
224 Southern Ocean cooling of the ACR (Pedro et al., 2018). The northern warming is abrupt (decadal  
225 scale) because it is associated with breakdown of stratification, release of accumulated sub-surface  
226 heat and rapid sea ice retreat in the North Atlantic and Nordic seas (Dokken et al., 2016; Sadatzki et  
227 al., 2018, Capron et al., 2021). The large-scale atmospheric counterpart to these changes stems from  
228 the effective northward shift of the thermal equator, which sets the position of the Hadley circulation  
229 and ITCZ. In shifting north, the cross equatorial Hadley cell gathers more energy from the warmer  
230 (northern) hemisphere for redistribution to the cooler (southern) hemisphere (Hartman et al., 2016),  
231 i.e. the dynamic atmospheric response acts to reduce the thermal imbalance between the  
232 hemispheres (see e.g. Fig 4 of Pedro et al. 2018). As detailed by Ceppi et al., (2013), and noted earlier,  
233 the northward shift of the westerlies occurs because a stronger cross-equatorial Hadley circulation  
234 also fluxes more momentum into the southern hemisphere subtropics, causing northward  
235 intensification of the eddy-driven jet and its surface expression in the southern westerlies.

236 An alternative hypothesis to the above 'extended thermal seesaw' was recently proposed by Denton  
237 et al, (2021). In their 'Zealandia Switch', orbitally-forced changes in southern hemisphere insolation  
238 drive millennial-scale variability in the position of the southern westerlies. When combined with the  
239 physical constraints of the Australian/Zealandia bathymetric footprint, these wind changes are

240 proposed to affect the global heat budget through the regulation of heat transport from the Tropical  
241 Pacific into the northern and southern hemisphere. We cannot exclude that this mechanism  
242 contributes to SH cooling during the ACR. However, the extended thermal seesaw framework, has the  
243 advantages of satisfying the north-south timing, amplitude and spatial pattern of observed millennial  
244 scale climate variations in multiple data compilations and data—model comparisons [e.g. Menviel et  
245 al., 2011; Pedro et al., 2016; Buizert et al., 2018, Corrick et al., 2020; Anderson et al., 2021, Capron et  
246 al., 2021]. Whether the ‘Zealandia Switch’ hypothesis satisfies such tests remains to be elucidated.

247 The northward shift of the southern westerlies during the ACR is synchronous with a reduction in  
248 Southern Ocean upwelling inferred from opal burial rates at TN057-13-4PC situated at 53°S, 5°E and  
249 with a CO<sub>2</sub> plateau in Antarctic ice cores (Figure 3i). Similarly, our evidence for southward shifted  
250 westerlies during the periods of deglacial warming that bracket the ACR aligns with increases in  
251 inferred Southern Ocean upwelling and intervals of CO<sub>2</sub> rise (Figure 3g,h). These results are consistent  
252 with the hypothesis that the position of the southern westerlies contributed to the observed deglacial  
253 CO<sub>2</sub> trends (Anderson et al., 2009; Toggweiler et al., 2006, Rae et al., 2018, Allen et al., 2019): i.e.  
254 enhanced Southern Ocean upwelling contributing to CO<sub>2</sub> outgassing when the winds were shifted  
255 southward toward Drake Passage and reduced outgassing when the winds shifted back northward,  
256 intensifying over Tasmania, during the ACR.

257

258

259 **References**

- 260 Anderson, R.F., Ali, S., Bratmiller, L.I., Nielsen, S.H.H., Fleisher, M.Q., Anderson, B.E., Burkle, L.H.,  
261 2009. Wind-Driven Upwelling in the Southern Ocean and the Deglacial Rise in Atmospheric CO<sub>2</sub>.  
262 *Science* 323, 1443-1448.
- 263 Allen, K.A., Sikes, E.L., Anderson, R.F., Rosenthal, Y., 2020. Rapid Loss of CO<sub>2</sub> From the South  
264 Pacific Ocean During the Last Glacial Termination. *Paleoceanography and Paleoclimatology* 35,  
265 e2019PA003766.
- 266 Anderson H.J., J.B. Pedro, H.C. Bostock, Z. Chase, T.L. Noble, 2021. Southern Ocean Sea Surface  
267 Temperature Response to Millennial-Scale Climate Change During Marine Isotope Stage 3: A  
268 Compilation. *Quaternary Science Reviews* 255, 106821,  
269 <https://doi.org/10.1016/j.quascirev.2021.106821>.
- 270 Ayliffe, L.K., Gagan, M.K., Zhao, J.-x., Drysdale, R.N., Hellstrom, J.C., Hantoro, W.S., Griffiths, M.L.,  
271 Scott-Gagan, H., St Pierre, E., Cowley, J.A., 2013. Rapid interhemispheric climate links via the  
272 Australasian monsoon during the last deglaciation. *Nature Communications* 4.
- 273 Blaauw, M., Christen, J.A., 2011. Flexible paleoclimate age-depth models using an autoregressive  
274 gamma process. *Bayesian Analysis* 6, 457-474.
- 275 Blarquez, O., Vanni re, B., Marlon, J.R., Daniau, A.-L., Power, M.J., Brewer, S., Bartlein, P.J., 2014.  
276 paleofire: an R package to analyse sedimentary charcoal records from the Global Charcoal Database  
277 to reconstruct past biomass burning. *Computers & Geosciences* 72, 255-261.
- 278 Bowman, D.M.J.S., Brown, M.J., 1986. Bushfires in Tasmania: a botanical approach to  
279 anthropological questions. *Archaeology in Oceania* 21, 166-171.
- 280 Box, G.E., Cox, D.R., 1964. An analysis of transformations. *Journal of the Royal Statistical Society:*  
281 *Series B (Methodological)* 26, 211-243.
- 282 Buizert, C., Sigl, M., Severi, M., Markle, B.R., Wettstein, J.J., McConnell, J.R., Pedro, J.B., Sodemann,  
283 H., Goto-Azuma, K., Kawamura, K., 2018. Abrupt ice-age shifts in southern westerly winds and  
284 Antarctic climate forced from the north. *Nature* 563, 681.
- 285 Capron, E., S.O. Rasmussen, T. J. Popp, T. Erhardt, H. Fischer, A. Landais, J.B. Pedro, G. Vettoretti,  
286 A. Grinsted, V. Gkinis, B. Vaughn, A. Svensson, B. M. Vinther, J. W. C. White. 2021. Multiple  
287 expressions in the anatomy of past abrupt warmings recorded in Greenland ice, *Nature*  
288 *Communications* 12:2106, 2021, <https://doi.org/10.1038/s41467-021-22241-w>.
- 289 Ceppi, P., Hwang, Y.T., Liu, X., Frierson, D.M., Hartmann, D.L., 2013. The relationship between the  
290 ITCZ and the Southern Hemispheric eddy-driven jet. *Journal of Geophysical Research: Atmospheres*  
291 118, 5136-5146.
- 292 Cirano, M., Middleton, J.F., 2004. Aspects of the mean wintertime circulation along Australia's  
293 southern shelves: Numerical studies. *Journal of Physical Oceanography* 34, 668-684.
- 294 Chiang, J.C.H., Lee, S.-Y., Putnam, A.E., Wang, X., 2014. South Pacific Split Jet, ITCZ shifts, and  
295 atmospheric North-South linkages during abrupt climate changes of the last glacial period. *Earth and*  
296 *Planetary Science Letters* 406, 233-246.  
297
- 298 Cleveland, W.S., 1979. Robust locally weighted regression and smoothing scatterplots. *Journal of the*  
299 *American statistical association* 74, 829-836.

- 300 Cohen, A.S., 2003. Paleolimnology: the history and evolution of lake systems. Oxford University  
301 Press.
- 302 Colhoun, E.A., 2000. Vegetation and climate during the last interglacial–glacial cycle in western  
303 Tasmania, Australia. *Palaeogeography, Palaeoclimatology, Palaeoecology* 155, 195-209.
- 304 Corrick E.C., R.N. Drysdale, J.C. Hellstrom, E. Capron, S.O. Rasmussen, X. Zhang, D. Fleitmann, I.  
305 Couchoud, E. Wolff. 2020. Synchronous timing of abrupt climate changes during the last glacial  
306 period, *Science* 369, 963–969, 10.1126/science.aay5538.
- 307 Croudace, I.W., Rothwell, R.G., 2015. *Micro-XRF Studies of Sediment Cores: Applications of a non-*  
308 *destructive tool for the environmental sciences.* Springer.
- 309 Daniau, A.L., Bartlein, P.J., Harrison, S., Prentice, I.C., Brewer, S., Friedlingstein, P., Harrison-Prentice,  
310 T., Inoue, J., Izumi, K., Marlon, J., 2012. Predictability of biomass burning in response to climate  
311 changes. *Global Biogeochemical Cycles* 26.
- 312 De Deckker, P., Moros, M., Perner, K., Jansen, E., 2012. Influence of the tropics and southern  
313 westerlies on glacial interhemispheric asymmetry. *Nature Geoscience* 5, 266-269.
- 314 Denniston, R.F., Wyrwoll, K.-H., Polyak, V.J., Brown, J.R., Asmerom, Y., Wanamaker, A.D., LaPointe,  
315 Z., Ellerbroek, R., Barthelmes, M., Cleary, D., 2013. A Stalagmite record of Holocene Indonesian–  
316 Australian summer monsoon variability from the Australian tropics. *Quaternary Science Reviews* 78,  
317 155-168.
- 318 Denton, G.H., Anderson, R.F., Toggweiler, J.R., Edwards, R.L., Schaefer, J.M., Putnam, A.E., 2010. The  
319 Last Glacial Termination. *Science* 328, 1652.
- 320 Denton, G.H., Putnam, A.E., Russell, J.L., Barrell, D.J., Schaefer, J.M., Kaplan, M.R., Strand, P.D., 2021.  
321 The Zealandia Switch: Ice age climate shifts viewed from Southern Hemisphere moraines.  
322 *Quaternary Science Reviews* 257, 106771.
- 323 Eugster, H.P., Hardie, L.A., 1978. *Saline lakes, lakes.* Springer, pp. 237-293.
- 324 Faegri, K., Iversen, J., 1989. *Textbook of pollen analysis.* Wiley, New York.
- 325 Fletcher, M.-S., Moreno, P.I., 2012. Have the Southern Westerlies changed in a zonally symmetric  
326 manner over the last 14,000 years? A hemisphere-wide take on a controversial problem. *Quaternary*  
327 *International* 253, 32–46.
- 328 Fletcher, M.-S., Thomas, I., 2007. Modern pollen–vegetation relationships in western Tasmania,  
329 Australia. *Review of Palaeobotany and Palynology* 146, 146-168.
- 330 Fletcher, M.-S., Thomas, I., 2010. A quantitative Late Quaternary temperature reconstruction from  
331 western Tasmania, Australia. *Quaternary Science Reviews* 29, 2351-2361.
- 332 Fletcher, M.-S., Wolfe, B.B., Whitlock, C., Pompeani, D.P., Heijnis, H., Haberle, S.G., Gadd, P.S.,  
333 Bowman, D.M.J.S., 2014. The legacy of mid-Holocene fire on a Tasmanian montane landscape.  
334 *Journal of Biogeography* 41, 476-488.
- 335 Garreaud, R.D., 2007. Precipitation and circulation covariability in the extratropics. *Journal of*  
336 *Climate* 20, 4789-4797.

- 337 Garreaud, R.D., Vuille, M., Compagnucci, R., Marengo, J., 2009. Present-day South American climate.  
338 *Palaeogeography Palaeoclimatology Palaeoecology* 281, 180-195.
- 339 Gillett, N.P., Kell, T.D., Jones, P.D., 2006. Regional climate impacts of the Southern Annular Mode.  
340 *Geophysical Research Letters* 33, L23704.
- 341 Haberzettl, T., Corbella, H., Fey, M., Janssen, S., Lucke, A., Mayr, C., Ohlendorf, C., Schabitz, F.,  
342 Schleser, G.H., Wille, M., 2007. Lateglacial and Holocene wet–dry cycles in southern Patagonia:  
343 chronology, sedimentology and geochemistry of a lacustrine record from Laguna Potrok Aike,  
344 Argentina. *The Holocene* 17, 297.
- 345 Hartmann, D., 2016. *Global Physical Climatology, Second Edition*. Elsevier, Amsterdam, Netherlands,  
346 485pp.
- 347 Hogg, A.G., Heaton, T.J., Hua, Q., Palmer, J.G., Turney, C.S., Southon, J., Bayliss, A., Blackwell, P.G.,  
348 Boswijk, G., Ramsey, C.B., 2020. SHCal20 Southern Hemisphere calibration, 0–55,000 years cal BP.  
349 *Radiocarbon*, 1-20.
- 350 Kelts, K., Hsü, K., 1978. *Freshwater carbonate sedimentation, Lakes*. Springer, pp. 295-323.
- 351 Koffman, T.N., Schaefer, J.M., Putnam, A.E., Denton, G.H., Barrell, D.J., Rowan, A.V., Finkel, R.C.,  
352 Rood, D.H., Schwartz, R., Plummer, M.A., 2017. A beryllium-10 chronology of late-glacial moraines in  
353 the upper Rakaia valley, Southern Alps, New Zealand supports Southern-Hemisphere warming  
354 during the Younger Dryas. *Quaternary Science Reviews* 170, 14-25.
- 355 Kunsch, H.R., 1989. The jackknife and the bootstrap for general stationary observations. *The annals*  
356 *of Statistics*, 1217-1241.
- 357 Kylander, M.E., Ampel, L., Wohlfarth, B., Veres, D., 2011. High-resolution X-ray fluorescence core  
358 scanning analysis of Les Echets (France) sedimentary sequence: new insights from chemical proxies.  
359 *Journal of Quaternary Science* 26, 109-117.
- 360 Lee, S.Y., Chiang, J.C., Matsumoto, K., Tokos, K.S., 2011. Southern Ocean wind response to North  
361 Atlantic cooling and the rise in atmospheric CO<sub>2</sub>: Modeling perspective and paleoceanographic  
362 implications. *Paleoceanography* 26.
- 363 Mariani, M., Fletcher, M.-S., 2017. Long-term climate dynamics in the extra-tropics of the South  
364 Pacific revealed from sedimentary charcoal analysis. *Quaternary Science Reviews* 173, 181-192.
- 365 Mariani, M., Fletcher, M.-S., Drysdale, R.N., Saunders, K.M., Heijnis, H., Jacobsen, G., Zawadzki, A.,  
366 2018. Coupling of the Intertropical Convergence Zone and Southern Hemisphere mid-latitude  
367 climate during the early to mid-Holocene. *Geology*.
- 368 Mariani, M., Fletcher, M.S., 2016. The Southern Annular Mode determines inter-annual and  
369 centennial-scale fire activity in temperate southwest Tasmania, Australia. *Geophysical Research*  
370 *Letters* 43.
- 371 Markle, B.R., Steig, E.J., Buizert, C., Schoenemann, S.W., Bitz, C.M., Fudge, T., Pedro, J.B., Ding, Q.,  
372 Jones, T.R., White, J.W., 2017. Global atmospheric teleconnections during Dansgaard-Oeschger  
373 events. *Nature Geoscience* 10, 36-40.

374 Marlon, J.R., Bartlein, P.J., Carcaillet, C., Gavin, D.G., Harrison, S.P., Higuera, P.E., Joos, F., Power, M.,  
375 Prentice, I., 2008. Climate and human influences on global biomass burning over the past two  
376 millennia. *Nature Geoscience* 1, 697-702.

377 McManus, J.F., Francois, R., Gherardi, J.M., Keigwin, L.D., Brown-Leger, S., 2004. Collapse and rapid  
378 resumption of Atlantic meridional circulation linked to deglacial climate changes. *Nature* 428, 834.

379 McWethy, D., Higuera, P., Whitlock, C., Veblen, T., Bowman, D., Cary, G., Haberle, S., Keane, R.,  
380 Maxwell, B., McGlone, M., 2013. A conceptual framework for predicting temperate ecosystem  
381 sensitivity to human impacts on fire regimes. *Global Ecology and Biogeography* 22, 900-912.

382 Menviel, L., Timmermann, A., Elison Timm, O., Mouchet A., 2011. Deconstructing the Last Glacial  
383 termination: the role of millennial and orbital-scale forcings, *Quaternary Science Reviews*, 30, 1155-  
384 1172, doi:10.1016/j.quascirev.2011.02.005.

385 Montade, V., Kageyama, M., Combourieu-Nebout, N., Ledru, M.-P., Michel, E., Siani, G., Kissel, C.,  
386 2015. Teleconnection between the Intertropical Convergence Zone and southern westerly winds  
387 throughout the last deglaciation. *Geology* 43, 735-738.

388 Pedro, J.B., Bostock, H.C., Bitz, C.M., He, F., Vandergoes, M.J., Steig, E.J., Chase, B.M., Krause, C.E.,  
389 Rasmussen, S.O., Markle, B.R., 2016. The spatial extent and dynamics of the Antarctic Cold Reversal.  
390 *Nature Geoscience* 9, 51-55.

391 Putnam, A.E., Denton, G.H., Schaefer, J.M., Barrell, D.J., Andersen, B.G., Finkel, R.C., Schwartz, R.,  
392 Doughty, A.M., Kaplan, M.R., Schlüchter, C., 2010. Glacier advance in southern middle-latitudes  
393 during the Antarctic Cold Reversal. *Nature Geoscience* 3, 700-704.

394 Rae, J.W.B., Burke, A., Robinson, L.F. et al. CO<sub>2</sub> storage and release in the deep Southern Ocean  
395 on millennial to centennial timescales. *Nature* 562, 569–573 (2018). [https://doi.org/10.1038/s41586-](https://doi.org/10.1038/s41586-018-0614-0)  
396 018-0614-0

397 Sadatzki, H., et al., 2019. Sea ice variability in the southern Norwegian Sea during glacial Dansgaard-  
398 Oeschger climate cycles. *Sci. Adv.* 5, eaau6174, doi: 10.1126/sciadv.aau6174.

399 Siani, G., Michel, E., De Pol-Holz, R., DeVries, T., Lamy, F., Carel, M., Isguder, G., Dewilde, F.,  
400 Lourantou, A., 2013. Carbon isotope records reveal precise timing of enhanced Southern Ocean  
401 upwelling during the last deglaciation. *Nature Communications* 4, 2758.

402 Sigman, D.M., Fripiat, F., Studer, A.S., Kemeny, P.C., Martínez-García, A., Hain, M.P., Ai, X., Wang, X.,  
403 Ren, H., Haug, G.H., 2020. The Southern Ocean during the ice ages: A review of the Antarctic surface  
404 isolation hypothesis, with comparison to the North Pacific. *Quaternary Science Reviews*, 106732.

405 Styger, J., Kirkpatrick, J.B., 2015. Less than 50 millimetres of rainfall in the previous month predicts  
406 fire in Tasmanian rainforest. *Papers and Proceedings of the Royal Society of Tasmania* 149, 1-5.

407 Toggweiler, J.R., Russell, J.L., Carson, S.R., 2006. Midlatitude westerlies, atmospheric CO<sub>2</sub>, and  
408 climate change during the ice ages. *Paleoceanography* 21, PA2005.

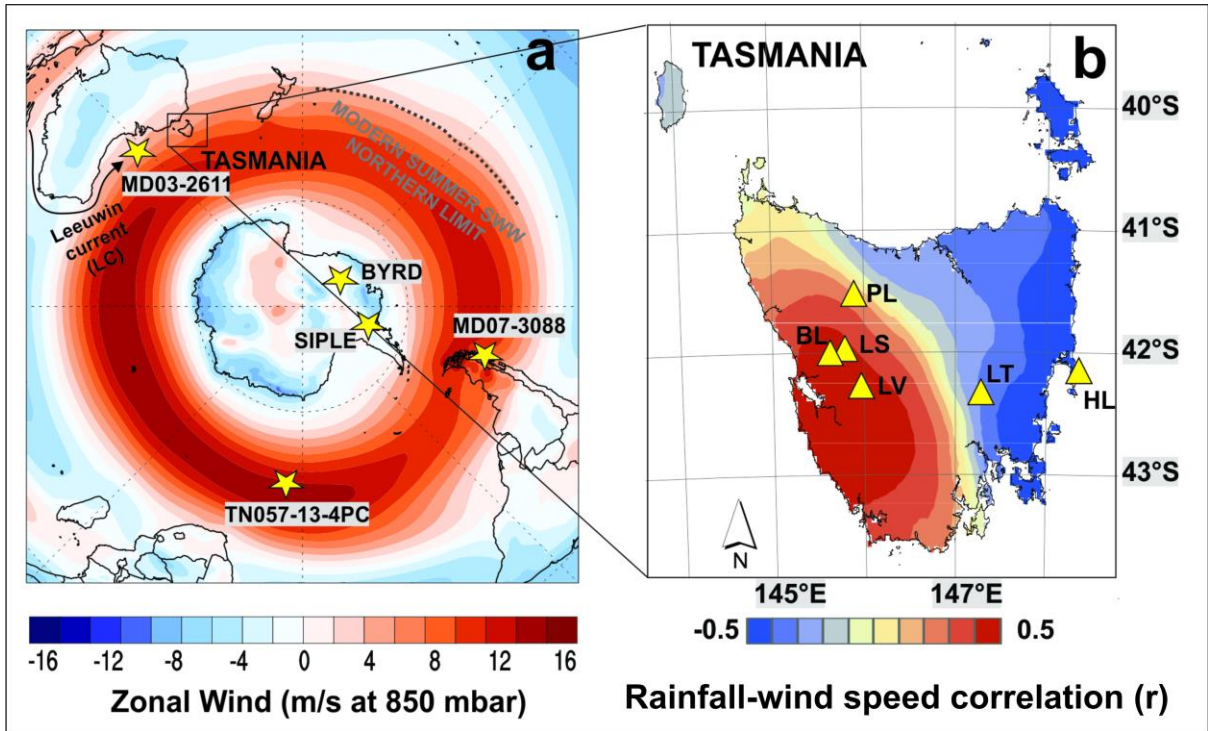
409 Vandergoes, M.J., Dieffenbacher-Krall, A.C., Newnham, R.M., Denton, G.H., Blaauw, M., 2008.  
410 Cooling and changing seasonality in the Southern Alps, New Zealand during the Antarctic Cold  
411 Reversal. *Quaternary Science Reviews* 27, 589-601.

412 Weaver, A.J., Middleton, J.H., 1989. On the dynamics of the Leeuwin Current. *Journal of Physical*  
413 *Oceanography* 19, 626-648.

414

415





416

417 Figure 1 (a) A map of zonal (southern westerly) wind speed showing the location of proxy sites  
 418 mentioned in the text and (b) a correlation map of southern westerly wind speed and rainfall in  
 419 Tasmania with sites analysed in this study: LV – Lake Vera; BL – Basin Lake; LS – Lake Selina; PL –  
 420 Paddy’s Lake; LT – Lake Tiberias and HL – Hazards Lagoon.

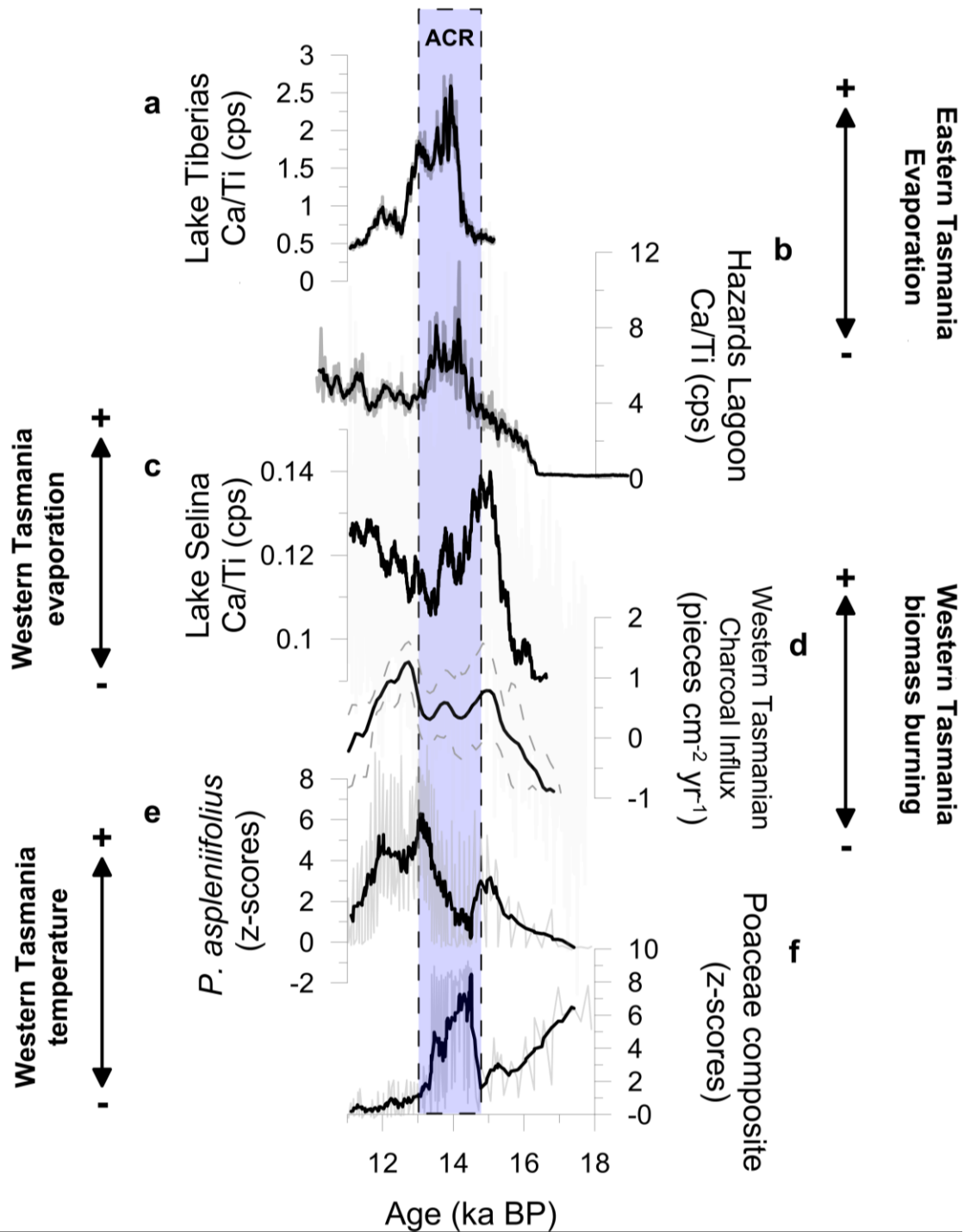
421

422

423

424

425

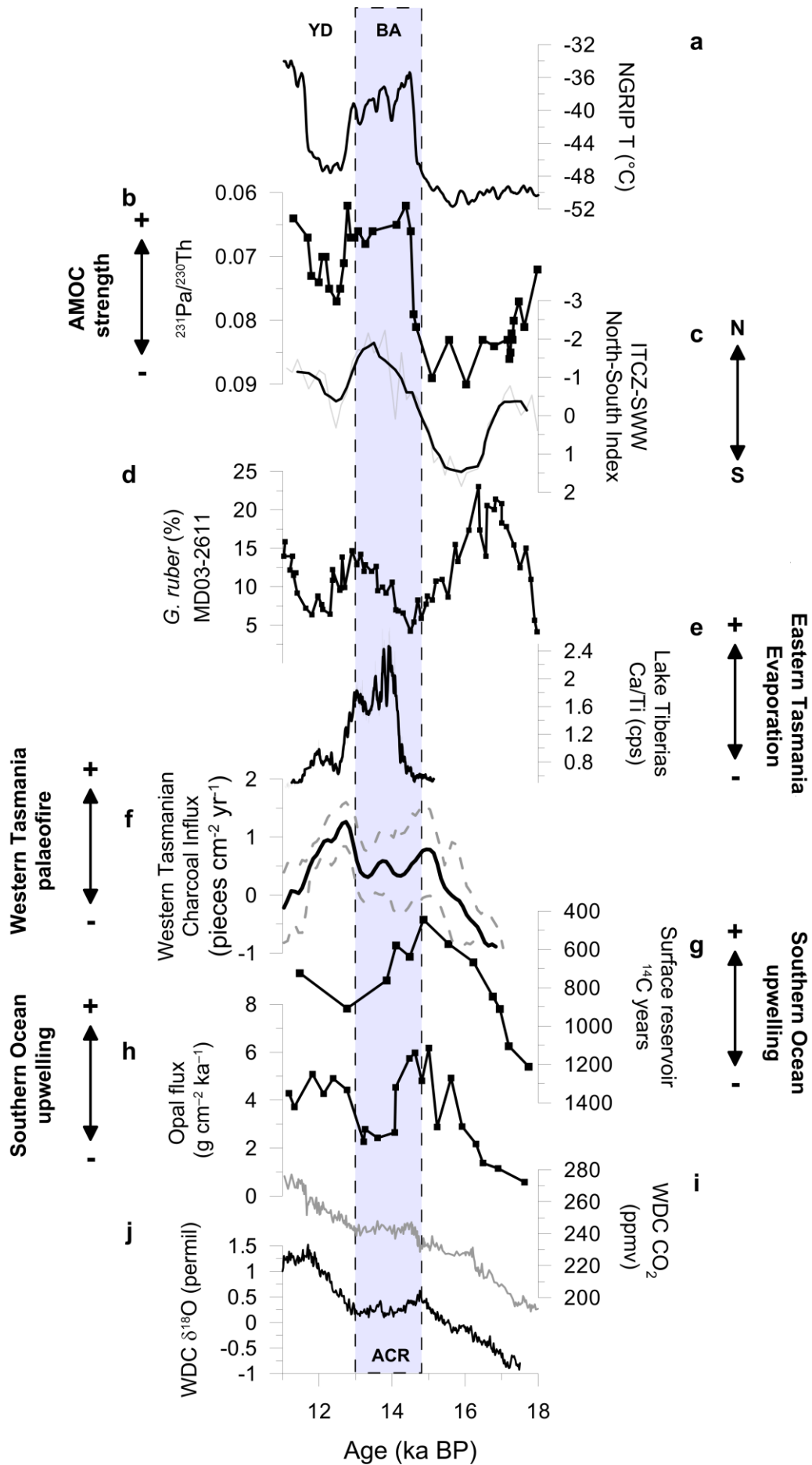


426

427 Figure 2 Proxy data spanning the period between 18-11 ka BP showing (a) Lake Tiberias and (b)  
 428 Hazards Lagoon and (c) Lake Selina Ca/Ti ratio, indicating changes in evaporite deposition. Black  
 429 curves indicate the weighted average (5-year window) for (a), (b) and weighted average (43-year  
 430 window) for (c); (d) western Tasmania charcoal influx composite (n=3) showing upper and lower  
 431 confidence intervals (dashed grey lines) indicating moisture-driven changes in fire activity; (e)

432 composite pollen (n=6) of the hygrophilous rainforest tree *Phyllocladus aspleniifolius*; and (f)  
433 composite Poaceae pollen curve (n=6) indicating changes in the grassland component of western  
434 Tasmanian pollen records. Black curves for both (e) and (f) indicate the weighted average (7-year  
435 window). Chronologies and associated uncertainties for all records used to create composite curves  
436 are presented in Supplementary Table 1 and Supplementary Figure 3.

437



439 **Figure 3 Global proxy data spanning the period between 18-11 ka showing (a) Proxy NGRIP surface-**  
440 **air temperature ( $^{15}\text{N}$  and diffusion-based reconstruction) (Buizert et al., 2018); (b) Proxy AMOC**  
441 **strength ( $^{231}\text{Pa}/^{230}\text{Th}$ ) from the Bermuda Rise (McManus et al., 2004); (c) Normalized index**  
442 **summarizing common latitudinal shifts of both the ITCZ and the southern westerlies (Montade et**  
443 **al., 2015); (d) *Globigerinoides ruber* % from ocean core MD03-2611 at 37°S (De Deckker et al., 2012)**  
444 **a tropical foraminifera indicating changes in the strength of the Leeuwin Current; (e) Lake Tiberias**  
445 **Ca/Ti ratio showing changes in evaporation (this study); (f) western Tasmania charcoal influx**  
446 **composite (n=3) indicating moisture-driven changes in fire activity (this study); (g) radiocarbon**  
447 **surface reservoir age determined off the coast of Chile at 46°S (Siani et al., 2013) showing changes**  
448 **in wind-driven upwelling (De Deckker et al., 2012); (h) Southern Ocean Opal flux, a proxy for**  
449 **upwelling south of the Antarctic polar front from core TN057-13-4PC at 53°S showing changes in**  
450 **wind-driven upwelling (Anderson et al., 2009); and West Antarctic Ice Sheet Divide ice core (WDC)**  
451 **(i)  $\text{CO}_2$  and (j)  $\delta^{18}\text{O}$  (Buizert et al., 2018).**

452

453 **Funding:**

454 Australian Research Council grant DI110100019

455 Australian Research Council grant IN140100050

456 Australian Research Council grant IN170100062

457 Australian Research Council grant IN170100063

458

459 **Author contributions:**

460 Conceptualization: MSF

461 Methodology: MSF, MM, JAA, KB, PSG, HH

462 Investigation: MSF, MM, JAA, KB

463 Visualization: MSF, MM, KB, TH

464 Funding acquisition: MSF, ALP

465 Project administration: MSF

466 Supervision: MSF

467 Writing – original draft: MSF, JP

468 Writing – review & editing: MSF, JP, TH, MM, JA, KB, MB, DAH, HH, PSG, ALP

469

470 **Data and materials availability:**

471 All data will be made available upon request

472

473